Structural definition of a conserved neutralization epitope on HIV-1 gp120

Table of Contents

Page

Supplementary Table 1. Crystallization, data collection, and refinement statistics for conformationally constrained variants of gp120. ……. 2-3

Supplementary Table 2. Expression levels for conformationally constrained gp120 variants. …… 4

Supplementary Table 3. Thermodynamics of CD4 interaction with conformationally constrained gp120 variants. …… 5

Supplementary Table 4A and 4B. Binding kinetics of CD4 and gp120-reactive antibodies to conformationally constrained gp120 variants as determined by surface-plasmon resonance. …….. 6-10

Supplementary Table 5. X-ray crystallographic data and refinement statistics for the antigen-binding fragment of b12 in complex with a stabilized gp120 core (Ds12F123). …….. 11

Supplementary Table 6. Interactive surface area with gp120 and effect of alanine substitution by residue of b12. …….. 12

Supplementary Table 7. Interactive surface areas of b12 and CD4 and effect of alanine substitution by residue of gp120. ……. 13-14

Supplementary Figure 1. Mutational stabilization of HIV-1 gp120 in its CD4-bound state. ……. 15-16

Supplementary Figure 2. Structural details of b12 complexed to an HIV-1 gp120 core. ……. 17-18

Supplementary Figure 3. Genomic analysis and sequence of b12. …….. 19

Supplementary Figure 4. gp120 sequence, secondary structure, contact residues, and structural differences between b12- and CD4-bound states. ……. 20-22

Supplementary Figure 5. Surface-plasmon resonance analysis of b12, CD4 and D1D2-Igαtp interactions with core and outer domain variants of gp120. ……. 22-24

Supplementary Figure 6. Model for CD4 engagement and effective antibody neutralization of HIV-1. …….. 25

Nomenclature for conformationally stabilized gp120 variants:

Cavity-altering substitutions are defined as: F1: M95W, F2: T257S/S375W; F3: A433M, and potential disulfide-bond cystine substitutions are: Ds1: W96C/V275C; Ds2: I109C/Q428C; Ds3: T123C/G431C; Ds4: K231C/E267C; Ds5: K231C/E268C.

Supplementary Table 1. Crystallization, data collection, and refinement statistics for conformationally constrained variants of gp120.

Crystal	Wild-type (S334A)[#]	F2	Ds1 F123
Crystallization			
Protein	8.5 mg/ml	9.0 mg/ml	9.0 mg/ml
Reservoir	7.0 % PEG 8000, 7.5 % 1,6-Hexanediol, 100 mM Na Citrate, pH 5.6	7.5 % PEG 4000, 8.5 % MPD, 100 mM Na Citrate, pH 5.6	7.5 % PEG 8000, 7.5 % MPD, 100 mM Na Citrate, pH 5.6
Data collection			
Space group	$P222_1$	$P222_1$	$P222_1$
Unit cell dimensions			
a, b, c (Å)	71.35, 88.10, 195.98	71.92, 88.13, 197.69	71.89, 87.31, 196.46
α, β, γ (°)	90.00, 90.00, 90.00	90.00, 90.00, 90.00	90.00, 90.00, 90.00
Wavelength, Å	0.9794	0.9794	1.0723
Resolution, Å	2.00	2.05	2.20
Completeness, %[*]	98.1 (91.3)	92.2 (68.2)	85.9 (59.5)
Redundancy	5.6 (2.2)	4.5 (2.1)	4.0 (3.6)
I/σ[*]	9.8 (1.1)	11.5 (1.1)	10.7 (1.6)
Rsym[*,†]	16.0 (73.5)	11.4 (50.5)	11.9 (41.0)
Refinement statistics (|F|>0 σ)			
Resolution, Å	2.00	2.05	2.20
R_{cryst}, %[‡]	18.1	20.6	20.2
R_{free}, %[‡,§]	23.1	24.4	24.2
Rmsd bond length, Å	0.005	0.009	0.005
Rmsd bond angles, °	0.916	0.997	0.893
Average B-factor, $Å^2$	30.8	25.9	49.7
Ramachandran analysis			
Favored, %	97.0	96.0	95.8
Allowed, %	100.0	99.7	99.9
PDB ID	2NXY	2NXZ	2NY0

Crystal	Ds2 F2	Ds3 F2	Ds4 F2
Crystallization			
Protein	4.0 mg/ml	6.0 mg/ml	3.7 mg/ml
Reservoir	7.5 % PEG 4000, 7.5 % MPD, 100 mM Na Citrate, pH 5.6	7.2 % PEG 8000, 7.8 % MPD, 100 mM Na Citrate, pH 5.6	8.5 % PEG 4000, 8.5 % MPD, 100 mM Na Citrate, pH 5.6
Data collection			
Space group	$P222_1$	$P222_1$	$P222_1$
Unit cell dimensions			
a, b, c (Å)	71.11, 88.16, 197.67	71.61, 88.02, 196.02	71.74, 88.20, 197.55
α, β, γ (°)	90.00, 90.00, 90.00	90.00, 90.00, 90.00	90.00, 90.00, 90.00
Wavelength, Å	0.9794	1.0000	0.9794
Resolution, Å	2.00	2.00	2.00
Completeness, %[*]	87.1 (63.2)	99.3 (94.4)	95.6 (85.9)
Redundancy	6.2 (3.0)	3.7 (3.4)	5.3 (2.6)
I/σ[*]	11.8 (1.1)	22.6 (2.9)	18.1 (1.7)
Rsym[*,†]	12.6 (58.0)	8.2 (37.4)	10.8 (49.6)
Refinement statistics (|F|>0 σ)			
Resolution, Å	2.00	2.00	2.00
R_{cryst}, %[‡]	20.9	19.4	20.3
R_{free}, %[‡,§]	25.0	22.3	24.3
Rmsd bond length, Å	0.006	0.005	0.009
Rmsd bond angles, °	1.007	0.911	0.962
Average B-factor, $Å^2$	33.7	44.8	33.0
Ramachandran analysis			
Favored, %	95.7	96.9	96.4
Allowed, %	99.9	100.0	99.8
PDB ID	2NY1	2NY2	2NY3

Crystal	Ds5 F2	Ds12 F123	Ds123 F12
Crystallization			
Protein	2.7 mg/ml	6.5 mg/ml	4.0 mg/ml
Reservoir	7.0 % PEG 8000, 8.0 % MPD, 100 mM Na Citrate, pH 5.6	9.2 % PEG 8000, 9.5 % MPD, 100 mM Na Citrate, pH 5.6	8.3 % PEG 8000, 7.4 % MPD, 100 mM Na Citrate, pH 5.6
Data collection			
Space group	$P222_1$	$P222_1$	$P222_1$
Unit cell dimensions			
a, b, c (Å)	70.96, 87.96, 196.18	73.26, 87.64, 197.33	72.31, 87.02, 196.08
α, β, γ (°)	90.00, 90.00, 90.00	90.00, 90.00, 90.00	90.00, 90.00, 90.00
Wavelength, Å	0.9794	0.9794	1.0000
Resolution, Å	2.00	2.50	2.80
Completeness, %*	97.9 (87.5)	84.9 (62.9)	92.5 (65.0)
Redundancy	6.1 (3.8)	3.9 (2.7)	3.4 (2.6)
I/σ*	18.1 (2.1)	11.3 (1.8)	9.4 (1.4)
Rsym*,†	12.5 (44.4)	16.3 (47.8)	15.1 (58.1)
Refinement statistics (|F|>0 σ)			
Resolution, Å	2.00	2.50	2.80
R_{cryst}, %‡	20.2	19.8	19.2
R_{free}, %‡,§	24.1	25.5	27.6
Rmsd bond length, Å	0.005	0.006	0.008
Rmsd bond angles, °	0.935	0.883	1.032
Average B-factor, $Å^2$	31.7	46.7	55.4
Ramachandran analysis			
Favored, %	96.5	96.0	89.9
Allowed, %	100.0	99.8	98.2
PDB ID	2NY4	2NY5	2NY6

* Values in parentheses are for the highest resolution shell.

† $R_{sym}=\Sigma|I-\langle I\rangle|/\Sigma\langle I\rangle$, where I is the observed intensity, and $\langle I\rangle$ is the average intensity of multiple observations of symmetry related reflections.

‡ $R=\Sigma_{hkl}||F_{obs}|-|F_{calc}||/\Sigma_{hkl}|F_{obs}|$

§ R_{free} calculated from 5% of the reflections excluded from refinement.

The nominal wild-type protein contained a S334A alteration, to ensure the absence of glycosylation at residue 332, the site of a lattice contact in these $P222_1$ crystals.

Supplementary Table 2. Expression level of conformationally constrained gp120 variants

gp120	Number of additional disulfide bonds (formed)	Expression level * (mg/L of cell culture supernatant)
WT core	0	7.5
F2	0	7.2
Ds5F2	0	7.0
Ds1F12	1	4.2
Ds1F123	1	6.6
Ds2F2	1	6.4
Ds3F2	1	6.6
Ds4F2	1	7.0
Ds12F123	2	4.6
Ds14F123	2	1.2
Ds24F2	2	0.9
Ds123F12	3	0.5
Ds123F123	3	0.3†
Ds124F123	3	<0.05†
Ds134F12	3	0.5†
Ds134F123	3	0.1†
Ds234F2	3	0.2†
Ds234F23	3	0.1†
Ds1234F12	4	<0.05†

* Expression levels were determined from the yield of purified gp120 by 17b-affinity chromatography.

† Expression levels for these gp120 variants were calculated from SPR sensorgrams of CD4 interacting with gp120 in cell-culture supernatants, assuming the CD4-gp120 association rate to be the same as the average CD4 on-rate shown in Table 1.

Supplementary Table 3. Thermodynamics of CD4 interaction with conformationally constrained gp120 variants.

gp120	ΔG (kcal mol^{-1})	ΔH (kcal mol^{-1})	-TΔS (kcal mol^{-1})
WT core	-9.97±0.03	-49.7±1.8	39.7±1.8
F2	-12.21±0.06	-51.3±1.8	39.1±1.8
Ds1F123	-10.48±0.16	-38.8±2.1	28.3±2.1
Ds2F2	-12.04±0.05	-29.3±1.0	17.2±1.0
Ds3F2	-12.55±0.10	-39.4±2.0	26.9±2.0
Ds4F2	-12.19±0.03	-46.4±2.3	34.2±2.3
Ds12F123	-11.53±0.08	-30.0±1.1	18.5±1.1
Ds123F12	-12.54±0.16	-31.4±1.6	18.9±1.6

Supplementary Table 4A. Binding kinetics of CD4 and CD4-induced antibodies to conformationally constrained gp120 variants as determined by surface-plasmon resonance.

gp120	CD4		
	on-rate ($M^{-1}s^{-1}$)	off-rate (s^{-1})	KD (M)
WT core	$2.52x10^{4}\pm2x10^{2}$	$1.30x10^{-3}\pm1x10^{-5}$	$5.16x10^{-8}\pm6x10^{-10}$
F2	$4.69x10^{4}\pm1\ x10^{2}$	$1.66x10^{-4}\pm5x10^{-6}$	$3.54x10^{-9}\pm1.1x10^{-10}$
Ds5F2	$4.67x10^{4}\pm1\ x10^{2}$	$1.18x10^{-4}\pm8x10^{-6}$	$2.53x10^{-9}\pm1.6x10^{-10}$
Ds2F2	$5.33x10^{4}\pm1\ x10^{2}$	$2.56x10^{-4}\pm7x10^{-6}$	$4.80x10^{-9}\pm1.4x10^{-10}$
Ds4F2	$4.50x10^{4}\pm1\ x10^{2}$	$1.26x10^{-4}\pm7x10^{-6}$	$2.80x10^{-9}\pm1.5x10^{-10}$
Ds3F2	$3.77x10^{4}\pm1\ x10^{2}$	$7.12x10^{-5}\pm4.5x10^{-6}$	$1.89x10^{-9}\pm1.2x10^{-10}$
Ds1F12	$3.46x10^{4}\pm1\ x10^{2}$	$3.49x10^{-4}\pm7x10^{-6}$	$1.01x10^{-8}\pm2x10^{-10}$
Ds1F123	$3.46x10^{4}\pm1\ x10^{2}$	$4.70x10^{-4}\pm8x10^{-6}$	$1.36x10^{-8}\pm2x10^{-10}$
Ds24F2	$3.44x10^{4}\pm1\ x10^{2}$	$3.21x10^{-4}\pm7x10^{-6}$	$9.33x10^{-9}\pm2.0x10^{-10}$
Ds14F123	$1.69x10^{4}\pm1\ x10^{2}$	$5.57x10^{-4}\pm7x10^{-6}$	$3.30x10^{-8}\pm4x10^{-10}$
Ds12F123	$4.90x10^{4}\pm2\ x10^{2}$	$4.93x10^{-4}\pm6x10^{-6}$	$1.01x10^{-8}\pm1x10^{-10}$
Ds123F12	$3.00x10^{4}\pm1\ x10^{2}$	$5.79x10^{-5}\pm6.1x10^{-6}$	$1.93x10^{-9}\pm2.0x10^{-10}$

gp120	17b		
	on-rate ($M^{-1}s^{-1}$)	off-rate (s^{-1})	KD (M)
WT core	$5.48x10^{3}\pm8.5\ x10^{2}$	$4.33x10^{-3}\pm4x10^{-5}$	$7.90x10^{-7}\pm1.22x10^{-7}$
F2	$2.93x10^{4}\pm8\ x10^{2}$	$1.55x10^{-2}\pm1x10^{-4}$	$5.29x10^{-7}\pm1.5x10^{-8}$
Ds5F2	$4.07x10^{4}\pm7\ x10^{2}$	$1.80x10^{-2}\pm1x10^{-4}$	$4.42x10^{-7}\pm7x10^{-9}$
Ds2F2	$1.05x10^{5}\pm\ 1x10^{3}$	$2.12x10^{-2}\pm1x10^{-4}$	$2.02x10^{-7}\pm1x10^{-9}$
Ds4F2	$2.27x10^{4}\pm6\ x10^{2}$	$1.85x10^{-2}\pm1x10^{-4}$	$8.15x10^{-7}\pm2.3x10^{-8}$
Ds3F2	$9.48x10^{4}\pm4\ x10^{2}$	$1.17x10^{-2}\pm2x10^{-5}$	$1.23x10^{-7}\pm1x10^{-9}$
Ds1F12	$1.61x10^{4}\pm6\ x10^{2}$	$1.61x10^{-2}\pm1x10^{-4}$	$1.00x10^{-6}\pm4x10^{-8}$
Ds1F123	$3.43x10^{4}\pm1.2\ x10^{3}$	$7.96x10^{-3}\pm9x10^{-5}$	$2.32x10^{-7}\pm8x10^{-9}$
Ds24F2	$5.66x10^{4}\pm6\ x10^{2}$	$2.07x10^{-2}\pm1x10^{-4}$	$3.66x10^{-7}\pm4x10^{-9}$
Ds14F123	$2.51x10^{4}\pm6\ x10^{2}$	$3.64x10^{-3}\pm4x10^{-5}$	$1.45x10^{-7}\pm4x10^{-9}$
Ds12F123	$3.73x10^{4}\pm5\ x10^{2}$	$1.19x10^{-2}\pm3x10^{-5}$	$3.19x10^{-7}\pm4x10^{-9}$
Ds123F12	$6.60x10^{5}\pm3\ x10^{3}$	$1.22x10^{-2}\pm2x10^{-5}$	$1.85x10^{-8}\pm1x10^{-10}$

gp120	m6		
	on-rate ($M^{-1}s^{-1}$)	off-rate (s^{-1})	KD (M)
WT core	$2.23x10^{4}\pm2.7x10^{3}$	$5.38x10^{-2}\pm1.5x10^{-3}$	$2.41x10^{-6}\pm3.0x10^{-7}$
F2	$1.43x10^{5}\pm9x10^{3}$	$9.82x10^{-2}\pm2.2x10^{-3}$	$6.87x10^{-7}\pm4.5x10^{-8}$
Ds5F2	$1.23x10^{5}\pm5x10^{3}$	$1.58x10^{-1}\pm3x10^{-3}$	$1.28x10^{-6}\pm6x10^{-8}$
Ds2F2	$3.23x10^{5}\pm1x10^{3}$	$1.28x10^{-1}\pm4x10^{-4}$	$3.96x10^{-7}\pm2x10^{-9}$
Ds4F2	$8.38x10^{4}\pm6.4x10^{3}$	$1.87x10^{-1}\pm4x10^{-3}$	$2.23x10^{-6}\pm1.8x10^{-7}$
Ds3F2	$2.28x10^{5}\pm2x10^{3}$	$5.03x10^{-2}\pm2x10^{-4}$	$2.21x10^{-7}\pm2x10^{-9}$
Ds1F12	$1.42x10^{5}\pm6x10^{3}$	$1.10x10^{-1}\pm3x10^{-3}$	$7.75x10^{-7}\pm3.9x10^{-8}$
Ds1F123	$1.17x10^{5}\pm1.2x10^{4}$	$5.72x10^{-2}\pm2.2x10^{-3}$	$4.89x10^{-7}\pm5.2x10^{-8}$
Ds24F2	$1.95x10^{5}\pm7x10^{3}$	$1.30x10^{-1}\pm2x10^{-3}$	$6.67x10^{-7}\pm2.7x10^{-8}$
Ds14F123	$1.28x10^{5}\pm5x10^{3}$	$5.95x10^{-3}\pm1.3x10^{-4}$	$4.65x10^{-8}\pm2.2x10^{-9}$
Ds12F123	$1.88x10^{5}\pm5x10^{3}$	$1.34x10^{-1}\pm2x10^{-3}$	$7.13x10^{-7}\pm2.3x10^{-8}$
Ds123F12	$1.42x10^{6}\pm1x10^{4}$	$4.61x10^{-2}\pm1x10^{-4}$	$3.25x10^{-8}\pm2x10^{-10}$

Supplementary Table 4B. Binding kinetics of CD4-binding-site and carbohydrate-recognizing antibodies to conformationally constrained gp120 variants as determined by surface-plasmon resonance.

gp120	b3		
	on-rate ($M^{-1}s^{-1}$)	off-rate (s^{-1})	KD (M)
WT core	$1.96x10^{5}$±1 $x10^{3}$	$1.06x10^{-4}$±$7x10^{-6}$	$5.41x10^{-10}$±$3.5x10^{-11}$
F2	$1.42x10^{5}$±3 $x10^{2}$	$7.44x10^{-5}$±$4.6x10^{-6}$	$5.24x10^{-10}$±$3.2x10^{-11}$
Ds5F2	$1.35x10^{5}$±2 $x10^{2}$	$7.96x10^{-5}$±$3.8x10^{-6}$	$5.90x10^{-10}$±$2.9x10^{-11}$
Ds2F2		No binding detected	
Ds4F2	$1.35x10^{5}$±3 $x10^{2}$	$7.55x10^{-5}$±$5.4x10^{-6}$	$5.59x10^{-10}$±$4.0x10^{-11}$
Ds3F2	$1.07x10^{5}$±3 $x10^{2}$	$8.01x10^{-5}$±$6.4x10^{-6}$	$7.49x10^{-10}$±$6.0x10^{-11}$
Ds1F12	$9.55x10^{4}$±2 $x10^{2}$	$1.74x10^{-4}$±$4x10^{-6}$	$1.82x10^{-9}$±$5x10^{-11}$
Ds1F123	$1.03x10^{5}$±4 $x10^{2}$	$1.91x10^{-4}$±$6x10^{-6}$	$1.85x10^{-9}$±$6x10^{-11}$
Ds24F2		No binding detected	
Ds14F123	$5.08x10^{4}$±$1x10^{2}$	$1.44x10^{-4}$±$4x10^{-6}$	$2.83x10^{-9}$±$8x10^{-11}$
Ds12F123		No binding detected	
Ds123F12		No binding detected	

gp120	b6		
	on-rate ($M^{-1}s^{-1}$)	off-rate (s^{-1})	KD (M)
WT core	$2.95x10^{5}$±$1x10^{3}$	$3.80x10^{-9}$±$5.0x10^{-10}$	$1.29x10^{-14}$±$1.7x10^{-15}$
F2	$2.47x10^{5}$±$1x10^{3}$	$6.97x10^{-5}$±$7.7x10^{-6}$	$2.82x10^{-10}$±$3.1x10^{-11}$
Ds5F2	$1.87x10^{5}$±$1x10^{3}$	$8.01x10^{-5}$±$8.5x10^{-6}$	$4.28x10^{-10}$±$4.5x10^{-11}$
Ds2F2		No binding detected	
Ds4F2	$2.15x10^{5}$±$1x10^{3}$	$5.70x10^{-5}$±$9.6x10^{-6}$	$2.65x10^{-10}$±$4.5x10^{-11}$
Ds3F2	$1.87x10^{5}$±$1x10^{3}$	$7.43x10^{-5}$±$5.8x10^{-6}$	$3.97x10^{-10}$±$3.1x10^{-11}$
Ds1F12	$1.66x10^{5}$±$1x10^{3}$	$1.44x10^{-4}$±$1.0x10^{-5}$	$8.67x10^{-10}$±$6.3x10^{-11}$
Ds1F123	$2.39x10^{5}$±$1x10^{3}$	$1.61x10^{-4}$±$6x10^{-6}$	$6.74x10^{-10}$±$2.7x10^{-11}$
Ds24F2		No binding detected	
Ds14F123	$1.68x10^{5}$±$1x10^{3}$	$1.09x10^{-4}$±$9x10^{-6}$	$6.49x10^{-10}$±$5.6x10^{-11}$
Ds12F123		No binding detected	
Ds123F12	$7.23x10^{3}$±$4.3x10^{2}$	$2.07x10^{-4}$±$2.5x10^{-5}$	$2.86x10^{-8}$±$3.7x10^{-9}$

gp120	b11		
	on-rate ($M^{-1}s^{-1}$)	off-rate (s^{-1})	KD (M)
WT core	$3.91x10^{4}$±$3x10^{2}$	$4.09x10^{-7}$±$5.0x10^{-6}$	$1.05x10^{-11}$±$1.3x10^{-10}$
F2	$3.05x10^{4}$±2 $x10^{2}$	$2.03x10^{-4}$±$1.2x10^{-5}$	$6.66x10^{-9}$±$3.8x10^{-10}$
Ds5F2	$2.85x10^{4}$±1 $x10^{2}$	$2.12x10^{-4}$±$1.1x10^{-5}$	$7.44x10^{-9}$±$3.7x10^{-10}$
Ds2F2		No binding detected	
Ds4F2	$2.78x10^{4}$±2 $x10^{2}$	$1.79x10^{-4}$±$1.4x10^{-5}$	$6.44x10^{-9}$±$4.9x10^{-10}$
Ds3F2	$2.91x10^{4}$±2 $x10^{2}$	$1.22x10^{-4}$±$1.1x10^{-5}$	$4.19x10^{-9}$±$3.9x10^{-10}$
Ds1F12	$2.13x10^{4}$±1 $x10^{2}$	$4.20x10^{-4}$±$1.1x10^{-5}$	$1.97x10^{-8}$±$5x10^{-10}$
Ds1F123	$3.34x10^{4}$±1 $x10^{2}$	$3.87x10^{-4}$±$1.1x10^{-5}$	$1.16x10^{-8}$±$3x10^{-10}$
Ds24F2		No binding detected	
Ds14F123	$2.43x10^{4}$±2 $x10^{2}$	$2.52x10^{-4}$±$1.6x10^{-5}$	$1.04x10^{-8}$±$7x10^{-10}$
Ds12F123		No binding detected	
Ds123F12		No binding detected	

gp120	b12		
	on-rate ($M^{-1}s^{-1}$)	off-rate (s^{-1})	KD (M)
WT core	$2.20x10^{5}\pm1x10^{3}$	$4.80x10^{-3}\pm1x10^{-5}$	$2.18x10^{-8}\pm1x10^{-10}$
F2	$1.57x10^{5}\pm2x10^{3}$	$1.22x10^{-2}\pm4x10^{-5}$	$7.77x10^{-8}\pm9x10^{-10}$
Ds5F2	$2.22x10^{5}\pm3x10^{3}$	$1.34x10^{-2}\pm1x10^{-4}$	$6.04x10^{-8}\pm1x10^{-9}$
Ds2F2	$1.68x10^{5}\pm8x10^{3}$	$4.31x10^{-2}\pm8x10^{-4}$	$2.57x10^{-7}\pm1.3x10^{-8}$
Ds4F2	$1.72x10^{5}\pm2x10^{3}$	$1.23x10^{-2}\pm1x10^{-4}$	$7.15x10^{-8}\pm9x10^{-10}$
Ds3F2	$1.93x10^{5}\pm3x10^{3}$	$1.01x10^{-2}\pm1x10^{-4}$	$5.23x10^{-8}\pm1x10^{-9}$
Ds1F12	$1.95x10^{5}\pm8x10^{3}$	$1.00x10^{-2}\pm1x10^{-4}$	$5.13x10^{-8}\pm2.2x10^{-9}$
Ds1F123	$2.08x10^{5}\pm1.0x10^{4}$	$1.06x10^{-2}\pm1x10^{-4}$	$5.10x10^{-8}\pm2.5x10^{-9}$
Ds24F2	$6.84x10^{4}\pm4.7x10^{3}$	$6.31x10^{-3}\pm1.9x10^{-4}$	$9.23x10^{-8}\pm6.9x10^{-9}$
Ds14F123	$1.72x10^{5}\pm7x10^{3}$	$6.70x10^{-3}\pm9x10^{-5}$	$3.90x10^{-8}\pm1.6x10^{-9}$
Ds12F123	$5.61x10^{4}\pm4.2x10^{3}$	$2.04x10^{-3}\pm5x10^{-5}$	$3.64x10^{-8}\pm2.9x10^{-9}$
Ds123F12	$4.34x10^{4}\pm1.1x10^{3}$	$8.33x10^{-4}\pm2.7x10^{-5}$	$1.92x10^{-8}\pm8x10^{-10}$

gp120	b13		
	on-rate ($M^{-1}s^{-1}$)	off-rate (s^{-1})	KD (M)
WT core	$5.14x10^{4}\pm2\ x10^{2}$	$6.43x10^{-4}\pm9x10^{-6}$	$1.25x10^{-8}\pm2x10^{-10}$
F2	$3.48x10^{4}\pm2\ x10^{2}$	$1.92x10^{-4}\pm9x10^{-6}$	$5.52x10^{-9}\pm2.6x10^{-10}$
Ds5F2	$3.15x10^{4}\pm1\ x10^{2}$	$1.91x10^{-4}\pm1.0x10^{-5}$	$6.06x10^{-9}\pm3.3x10^{-10}$
Ds2F2	$9.96x10^{3}\pm4.7\ x10^{2}$	$9.71x10^{-4}\pm4.5x10^{-5}$	$9.75x10^{-8}\pm6.4x10^{-9}$
Ds4F2	$2.98x10^{4}\pm1\ x10^{2}$	$2.14x10^{-4}\pm1x10^{-5}$	$7.18x10^{-9}\pm3.3x10^{-10}$
Ds3F2	$2.96x10^{4}\pm1\ x10^{2}$	$1.68x10^{-4}\pm8x10^{-6}$	$5.68x10^{-9}\pm2.8x10^{-10}$
Ds1F12	$2.51x10^{4}\pm1\ x10^{2}$	$1.86x10^{-4}\pm9x10^{-6}$	$7.41x10^{-9}\pm3.4x10^{-10}$
Ds1F123	$4.24x10^{4}\pm1\ x10^{2}$	$1.92x10^{-4}\pm8x10^{-6}$	$4.53x10^{-9}\pm2.0x10^{-10}$
Ds24F2	$1.06x10^{4}\pm6\ x10^{2}$	$1.68x10^{-3}\pm5x10^{-5}$	$1.58x10^{-7}\pm1x10^{-8}$
Ds14F123	$3.22x10^{4}\pm1\ x10^{2}$	$1.69x10^{-4}\pm1.2x10^{-5}$	$5.25x10^{-9}\pm3.6x10^{-10}$
Ds12F123	$4.75x10^{3}\pm3.8\ x10^{2}$	$1.38x10^{-3}\pm3x10^{-5}$	$2.91x10^{-7}\pm2.4x10^{-8}$
Ds123F12	$2.60x10^{3}\pm5.0\ x10^{2}$	$1.51x10^{-3}\pm6x10^{-5}$	$5.81x10^{-7}\pm1.14x10^{-7}$

gp120	m14		
	on-rate ($M^{-1}s^{-1}$)	off-rate (s^{-1})	KD (M)
WT core	$3.56x10^{5}\pm1\ x10^{3}$	$6.00x10^{-4}\pm4x10^{-6}$	$1.69x10^{-9}\pm1x10^{-11}$
F2	$1.64x10^{5}\pm2.3x10^{4}$	$5.67x10^{-2}\pm3x10^{-3}$	$3.46x10^{-7}\pm5.2x10^{-8}$
Ds5F2	$6.39x10^{2}\pm8.26\ x10^{2}$	$1.05x10^{-1}\pm7x10^{-3}$	$1.64x10^{-4}\pm2.13x10^{-4}$
Ds2F2		No binding detected	
Ds4F2	$1.73x10^{5}\pm2.5x10^{4}$	$1.21x10^{-1}\pm1.2x10^{-2}$	$6.99x10^{-7}\pm1.22x10^{-7}$
Ds3F2	$1.41x10^{5}\pm2.4x10^{4}$	$7.27x10^{-2}\pm7.3x10^{-3}$	$5.16x10^{-7}\pm1.01x10^{-7}$
Ds1F12	$8.95x10^{4}\pm9.2x10^{3}$	$7.42x10^{-2}\pm3.5x10^{-3}$	$8.29x10^{-7}\pm9.4x10^{-8}$
Ds1F123	$2.61x10^{5}\pm1.7x10^{4}$	$7.42x10^{-3}\pm2.4x10^{-4}$	$2.84x10^{-8}\pm2.1x10^{-9}$
Ds24F2	$1.75x10^{4}\pm1.15x10^{4}$	$3.87x10^{-2}\pm2.5x10^{-3}$	$2.21x10^{-6}\pm1.46x10^{-6}$
Ds14F123	$9.09x10^{4}\pm6.2x10^{3}$	$8.46x10^{-3}\pm2.6x10^{-4}$	$9.31x10^{-8}\pm6.9x10^{-9}$
Ds12F123		No binding detected	
Ds123F12		No binding detected	

gp120	m18		
	on-rate ($M^{-1}s^{-1}$)	off-rate (s^{-1})	KD (M)
WT core	$4.55x10^{5}\pm1x10^{3}$	$1.65x10^{-4}\pm5x10^{-6}$	$3.63x10^{-10}\pm1.1x10^{-11}$
F2	$2.26x10^{5}\pm1x10^{3}$	$2.85x10^{-4}\pm9x10^{-6}$	$1.26x10^{-9}\pm4x10^{-11}$
Ds5F2	$2.41x10^{5}\pm1x10^{3}$	$3.05x10^{-4}\pm7x10^{-6}$	$1.27x10^{-9}\pm3x10^{-11}$
Ds2F2	$7.57x10^{2}\pm2.42x10^{2}$	$1.87x10^{-3}\pm2x10^{-5}$	$2.47x10^{-6}\pm7.9x10^{-7}$
Ds4F2	$2.61x10^{5}\pm1x10^{3}$	$2.79x10^{-4}\pm6x10^{-6}$	$1.07x10^{-9}\pm2x10^{-11}$
Ds3F2	$2.46x10^{5}\pm1x10^{3}$	$3.19x10^{-4}\pm6x10^{-6}$	$1.30x10^{-9}\pm3x10^{-11}$
Ds1F12	$1.97x10^{5}\pm1x10^{3}$	$3.46x10^{-4}\pm6x10^{-6}$	$1.76x10^{-9}\pm3x10^{-11}$
Ds1F123	$2.00x10^{5}\pm1x10^{3}$	$3.50x10^{-4}\pm9x10^{-6}$	$1.75x10^{-9}\pm5x10^{-11}$
Ds24F2	$9.68x10^{1}\pm6.95\ x10^{1}$	$3.23x10^{-3}\pm2.4x10^{-4}$	$3.34x10^{-5}\pm2.41x10^{-5}$
Ds14F123	$1.04x10^{5}\pm5\ x10^{2}$	$3.64x10^{-4}\pm1x10^{-5}$	$3.50x10^{-9}\pm9x10^{-11}$
Ds12F123	$3.86x10^{4}\pm3.16x10^{3}$	$4.38x10^{-3}\pm1.4x10^{-4}$	$1.13x10^{-7}\pm1x10^{-8}$
Ds123F12	$4.08x10^{3}\pm5.2\ x10^{2}$	$5.67x10^{-4}\pm3.6x10^{-5}$	$1.39x10^{-7}\pm2.0x10^{-8}$

gp120	F91		
	on-rate ($M^{-1}s^{-1}$)	off-rate (s^{-1})	KD (M)
WT core	$1.96x10^{5}\pm1x10^{3}$	$1.40x10^{-4}\pm1x10^{-5}$	$7.14x10^{-10}\pm5.0x10^{-11}$
F2	$1.78x10^{5}\pm6x10^{3}$	$1.42x10^{-2}\pm2x10^{-4}$	$7.98x10^{-8}\pm2.\ 9x10^{-9}$
Ds5F2	$1.05x10^{5}\pm2x10^{3}$	$1.74x10^{-2}\pm1x10^{-4}$	$1.66x10^{-7}\pm3x10^{-9}$
Ds2F2		No binding detected	
Ds4F2	$1.41x10^{5}\pm5x10^{3}$	$1.62x10^{-2}\pm2x10^{-4}$	$1.15x10^{-7}\pm4x10^{-9}$
Ds3F2	$8.44x10^{4}\pm2.9x10^{3}$	$2.27x10^{-2}\pm3x10^{-4}$	$2.69x10^{-7}\pm1.0x10^{-8}$
Ds1F12	$1.15x10^{5}\pm2x10^{3}$	$2.02x10^{-2}\pm2x10^{-4}$	$1.76x10^{-7}\pm3x10^{-9}$
Ds1F123	$9.01x10^{4}\pm2.0x10^{3}$	$1.58x10^{-2}\pm2x10^{-4}$	$1.75x10^{-7}\pm4x10^{-9}$
Ds24F2		No binding detected	
Ds14F123	$3.47x10^{4}\pm1.4x10^{3}$	$1.38x10^{-2}\pm2x10^{-4}$	$3.98x10^{-7}\pm1.7x10^{-8}$
Ds12F123		No binding detected	
Ds123F12		No binding detected	

gp120	F105		
	on-rate ($M^{-1}s^{-1}$)	off-rate (s^{-1})	KD (M)
WT core*	$2.44x10^{5}\pm2x10^{3}$	$4.45x10^{-3}\pm2x10^{-5}$	$1.82x10^{-8}\pm2x10^{-10}$
F2		No binding detected	
Ds5F2		No binding detected	
Ds2F2		No binding detected	
Ds4F2		No binding detected	
Ds3F2		No binding detected	
Ds1F12		No binding detected	
Ds1F123		No binding detected	
Ds24F2		No binding detected	
Ds14F123		No binding detected	
Ds12F123		No binding detected	
Ds123F12		No binding detected	

gp120	15e		
	on-rate ($M^{-1}s^{-1}$)	off-rate (s^{-1})	KD (M)
WT core	$1.64x10^{5}$±4x 10^{2}	$1.79x10^{-4}$±$6x10^{-6}$	$1.09x10^{-9}$±$3x10^{-11}$
F2		No binding detected	
Ds5F2		No binding detected	
Ds2F2		No binding detected	
Ds4F2		No binding detected	
Ds3F2		No binding detected	
Ds1F12		No binding detected	
Ds1F123		No binding detected	
Ds24F2		No binding detected	
Ds14F123		No binding detected	
Ds12F123		No binding detected	
Ds123F12		No binding detected	

gp120	2G12		
	on-rate ($M^{-1}s^{-1}$)	off-rate (s^{-1})	KD (M)
WT core	$1.83x10^{5}$±1 $x10^{3}$	$1.08x10^{-3}$±$1x10^{-5}$	$5.90x10^{-9}$±$6x10^{-11}$
F2	$1.68x10^{5}$±1 $x10^{3}$	$1.06x10^{-3}$±$1x10^{-5}$	$6.31x10^{-9}$±$9x10^{-11}$
Ds5F2	$5.63x10^{4}$±3 $x10^{2}$	$9.55x10^{-4}$±$1.0x10^{-5}$	$1.70x10^{-8}$±$2x10^{-10}$
Ds2F2	$3.86x10^{4}$±4 $x10^{2}$	$1.13x10^{-3}$±$1x10^{-5}$	$2.93x10^{-8}$±$5x10^{-10}$
Ds4F2	$4.63x10^{4}$±4 $x10^{2}$	$1.09x10^{-3}$±$1x10^{-5}$	$2.35x10^{-8}$±$4x10^{-10}$
Ds3F2	$6.79x10^{4}$±2 $x10^{2}$	$1.10x10^{-3}$±$1x10^{-5}$	$1.62x10^{-8}$±$1x10^{-10}$
Ds1F12	$3.79x10^{4}$±2 $x10^{2}$	$1.17x10^{-3}$±$1x10^{-5}$	$3.09x10^{-8}$±$3x10^{-10}$
Ds1F123	$1.04x10^{5}$±1 $x10^{3}$	$1.18x10^{-3}$±$1x10^{-5}$	$1.13x10^{-8}$±$2x10^{-10}$
Ds24F2	$6.04x10^{4}$±4 $x10^{2}$	$1.12x10^{-3}$±$1x10^{-5}$	$1.85x10^{-8}$±$2x10^{-10}$
Ds14F123	$1.60x10^{5}$±$2x10^{3}$	$2.14x10^{-3}$±$3x10^{-5}$	$1.34x10^{-8}$±$2x10^{-10}$
Ds12F123	$5.71x10^{4}$±3 $x10^{2}$	$1.50x10^{-3}$±$1x10^{-5}$	$2.63x10^{-8}$±$2x10^{-10}$
Ds123F12	$9.16x10^{4}$±3 $x10^{2}$	$1.21x10^{-3}$±$1x10^{-5}$	$1.32x10^{-8}$±$1x10^{-10}$

The gp120-reactive ligand (CD4, antibody or Fab) was immobilized directly onto a CM5 sensor chip to a surface density of ~500 response units (RU) with standard amine coupling. Variant gp120s at 100-200 nM were passed over the modified sensor chips at 30 µl/min for 5 min, followed by a 5-min-dissociation phase to identify rough binding affinities, and then a 2-fold increasing series of gp120 concentrations were passed over the chip, with the concentration of the series adjusted so that at least three runs resulted in maximum RUs in the 10-150 RU range. The buffer in all experiments was 10 mM HEPES, pH 7.4, 150 mM NaCl, 3 mM EDTA, and 0.01% surfactant P-20. Sensorgrams were fit globally with BiaEvaluation 4.1 using a 1:1 Langmuir model of binding. Although CD4 and other ligands might formally be analyzed with a two-state binding model, such treatment should not affect the primary on-rates nor overall KDs reported here.

Supplementary Table 5. X-ray crystallographic data and refinement statistics for the antigen-binding fragment of b12 in complex with a stabilized gp120 core (Ds12F123).

Crystal	Ds12F123-gp120:b12 Fab
Data collection	
Space group	$P6_522$
Unit cell dimensions	
a, b, c (Å)	101.96, 101.96, 298.29
α, β, γ (°)	90.00, 90.00, 120.00
Wavelength, Å	1.0000
Resolution, Å	2.30
Completeness, %*	97.2 (77.5)
Redundancy	8.8 (2.3)
I/σ*	35.5 (1.2)
Rsym*,†	9.6 (75.5)
Refinement statistics (|F|>0 σ)	
Resolution, Å	2.30
R_{cryst}, %‡	19.3
R_{free}, %‡,§	25.5
Rmsd bond length, Å	0.004
Rmsd bond angles, °	0.852
Average B-factor, Å^2	75.9
Ramachandran analysis	
Favored, %	95.3
Allowed, %	99.7
PDB ID	2NY7

* Values in parentheses are for the highest resolution shell.

† $R_{sym}=\Sigma|I-\langle I\rangle|/\Sigma\langle I\rangle$, where I is the observed intensity, and $\langle I\rangle$ is the average intensity of multiple observations of symmetry related reflections.

‡ $R=\Sigma_{hkl}||F_{obs}|-|F_{calc}||/\Sigma_{hkl}|F_{obs}|$

§ R_{free} calculated from 5% of the reflections excluded from refinement.

Supplementary Table 6. Interactive surface area with gp120 and effect of alanine substitution by residue of b12.

b12 substitution residue	Interactive surface size		Apparent affinity for Ala*			
	Mainchain (Å^2)	Sidechain (Å^2)	JR-FL (%)	IIIB (%)	JR-CSF (%)	Ds12F123 (%)
Heavy chain						
N52	0.0	14.1	100	45	-	-
P52a	5.8	0.0	80	50	-	-
N56	4.2	18.7	90	140	-	-
V95	0.0	9.9	8.5	<3	-	-
G96	2.7	0.0	100	75	-	-
P97	2.2	5.5	60	40	-	-
Y98	17.4	67.3	<3	<3	<3	<3
S99	3.1	0.0	90	95	-	-
W100	18.0	98.0	5	5	5.5	<3
D100a	2.6	0.9	45	30	80	50
D100b	3.2	0.0	40	45	-	-
S100c	0.0	0.0	130	75	-	-
P100d	5.8	12.4	5	20	-	-
Q100e	6.1	5.2	<3	<3	-	-
D100f	0.0	0.0	30	15	-	-
N100g	0.0	15.5	<3	<3	-	-
Y100h	0.0	21.5	<3	<3	-	-
Y100i	0.0	0.0	<3	<3	-	-
M100j	0.0	0.0	150	150	-	-
D101	0.0	0.0	80	60	-	-
V102	0.0	0.0	110	80	-	-
Light chain						
S30	0.0	0.0	<3	<3	<3	<3

*Apparent affinities correspond to the concentration at half-maximal binding of the wild-type Fab over the mutant Fab. Data for isolates JR-FL and IIIB taken from Zwick et al, *J. Virol.* **77**, 5863-5876 (2003).

Supplementary Table 7. Interactive surface areas of b12 and CD4 and effect of alanine substitution by residue of gp120.

gp120 residue*	Interactive surface size†				Apparent affinity for Ala substitution‡	
	b12		CD4		b12	CD4§
	Main ($Å^2$)	Side ($Å^2$)	Main ($Å^2$)	Side ($Å^2$)	(%)	(%)
E87	0.0	0.0	0.0	0.0	7	114
M95	0.0	0.0	0.0	0.0	75	59
K97	0.0	0.0	0.0	0.0	134	50
E102	0.0	0.0	0.0	0.0	63	47
W112	0.0	0.0	0.0	0.0	2	67
D113	0.0	0.0	0.0	0.0	1	9
K121	0.0	0.0	0.0	0.0	4	3
L122	0.0	0.0	0.0	0.0	27	62
T123	0.0	0.0	0.0	0.0	233	42
L125	0.0	0.0	2.1	3.5	383	23
V127	0.0	0.0	5.0	26.4	62	26
I165	0.0	0.0	0.0	0.0	20	57
R166	0.0	0.0	0.0	0.0	52	44
K171	0.0	0.0	0.0	0.0	118	26
E172	0.0	0.0	0.0	0.0	143	93
F176	0.0	0.0	0.0	0.0	2	19
D180	0.0	0.0	0.0	0.0	1	31
I184	0.0	0.0	0.0	0.0	0.6	27
D185	0.0	0.0	0.0	0.0	6	62
T190	0.0	0.0	0.0	0.0	21	187
N197	0.0	0.0	0.0	0.0	25	3
T198	0.0	0.0	0.0	0.8	0.1	42
S199	0.0	0.0	0.0	0.0	123	4
T202	0.0	0.0	0.0	0.0	220	62
K207	0.0	0.0	0.0	0.0	2	5
F210	0.0	0.0	0.0	0.0	77	37
I213	0.0	0.0	0.0	0.0	20	31
R252	0.0	0.0	0.0	0.0	17	47
S256	1.2	0.0	0.0	0.0	13	47
T257	11.4	8.9	0.0	0.0	28	21
N262	0.0	0.0	0.0	0.0	6	5
R273	0.0	0.0	0.0	0.0	0.9	40
N276	0.0	0.0	0.0	0.0	225	27
D279	0.0	0.0	1.8	13.9	27	33
N280	12.0	5.6	11.1	33.0	75	44
K282	0.0	0.0	2.4	14.8	32	78
T283	0.0	0.0	1.1	16.9	55	53
Q337	0.0	0.0	0.0	0.0	83	122
K343	0.0	0.0	0.0	0.0	8	187
R350	0.0	0.0	0.0	0.0	6	43
S365	15.4	12.1	12.6	25.8	534	23
G366	33.2	0.0	18.8	0.0	9	1
G367	46.3	0.0	23.5	0.0	1	2
D368	7.7	33.8	6.2	46.6	15	1
P369	5.9	30.2	0.0	0.0	129	117
E370	7.8	10.1	0.0	18.0	0.2	4
I371	3.7	53.7	0.0	42.9	26	7
V372	0.0	28.6	0.0	0.0	4	52
M373	0.0	19.8	0.0	0.0	13	80
Y384	9.8	4.0	0.0	0.0	2	40
N386	7.3	24.8	0.0	0.0	11	26
T388	0.0	0.0	0.0	0.0	8	19
W395	0.0	0.0	0.0	0.0	18	23
K421	0.0	0.0	0.0	0.0	7	44
N425	0.0	0.0	7.3	24.5	80	11
M426	0.0	0.0	14.9	0.0	0.2	0.2
W427	0.0	0.0	16.6	10.1	21	9
V430	11.0	9.4	13.7	56.7	580	2
K432	0.0	29.3	0.0	3.8	7.5	50
I439	0.0	0.0	0.0	0.0	2	10
T450	0.0	0.0	0.0	0.0	7	16

T455	0.0	30.6	4.2	23.0	500	1
R456	11.4	0.0	8.4	0.0	6	53
D457	3.1	2.1	16.1	21.0	5	2
G458	1.5	0.0	2.4	0.0	300	2
G459	0.0	0.0	19.5	0.0	54	37
N461	0.0	0.0	0.0	0.0	4	160
E462	0.0	0.0	0.0	0.0	21	32
S463	0.0	0.0	0.0	0.0	50	53
I467	0.0	0.0	0.0	0.0	63	3
R469	0.0	0.0	0.0	18.2	1.4	8
P470	0.8	0.0	0.0	0.0	1.3	13
G471	1.4	0.0	0.0	0.0	37	89
G472	24.3	0.0	20.7	0.0	22	2
G473	34.8	0.0	25.3	0.0	998	2
D474	16.9	8.9	10.6	24.2	91	22
M475	15.7	29.5	0.0	5.1	130	64
R476	0.0	0.0	0.0	5.2	25	40
D477	0.0	0.0	0.0	7.6	2	187
W479	0.0	0.0	0.0	0.0	1.3	19
R480	0.0	0.0	0.0	0.0	37	73

* Amino acid identity is from JR-CSF, the HIV-1 isolate in which Ala substitutions were made [Pantophlet et al. *J. Virol.* **77**, 642-658 (2003)].

† Both b12 and CD4 interactive surfaces were calculated in the context of the Ds12F123 variant of the gp120 core.

‡ Apparent affinities correspond to the concentration at half-maximal binding of b12 or CD4-IgG2 against $gp120_{JR\text{-}CSF}$ divided by the concentration at half-maximal binding of b12 or CD4-IgG2 against the mutant gp120 [data from Pantophlet et al. *J. Virol.* **77**, 642-658 (2003)].

§ CD4-IgG2 was used as a surrogate for CD4.

Supplementary Figure 1

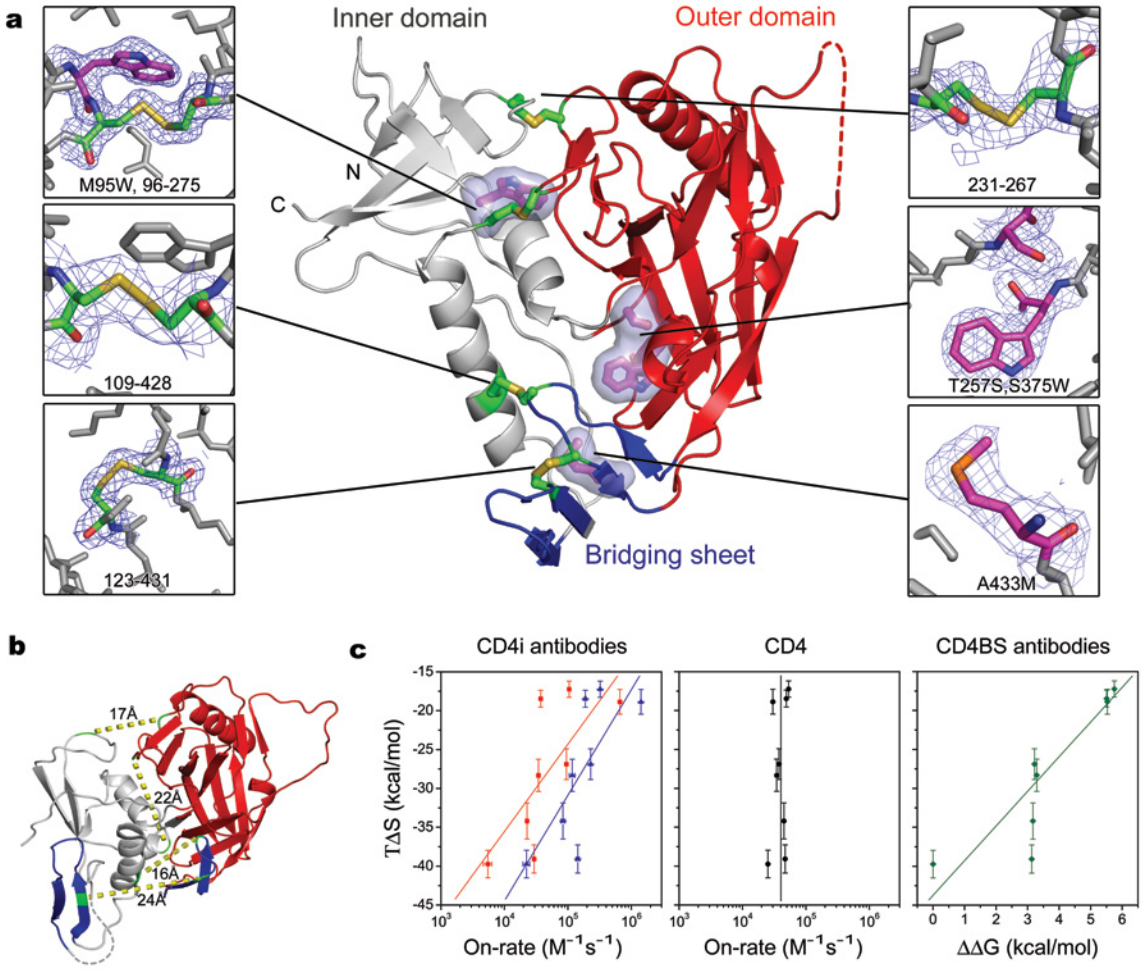

Supplementary Figure 1. Mutational stabilization of HIV-1 gp120 in its CD4-bound state.

The gp120 glycoprotein displays extraordinary conformational flexibility. To stabilize gp120 into the conformation it assumes when bound by CD4, we devised interdomain disulfides and cavity-altering substitutions. Alteration of an unusual interfacial pocket at the nexus of the inner domain, outer domain and bridging sheet through a S375W mutant was previously found to partially stabilize gp120 in its CD4-bound state [Xiang, S.H. et al. *J. Virol*. **76**, 9888-9899 (2002)], but we found this mutant prone to aggregate. An additional T257S change, however, resulted in well-behaved protein, and we were able to solve the structure of a S375W, T257S gp120 core bound to CD4 and Fab 17b at 2.0 Å (supplementary Table 1).

We analyzed Cβ-Cβ distances within the context of the S375W, T257S structure to construct novel interdomain disulfides. Molecular modeling suggested four interdomain disulfides could be made to

connect residues 96-275, 109-428, 231-267 and 231-268. The disulfide at 96-275 required a Trp 96 to Cys change that created a large cavity; we designed an additional M95W substitution to compensate. All four novel disulfides were constructed in the context of the S375W, T257S core. In addition, we tested a 123-431 disulfide that tied together the second and third strands of the bridging sheet as well as an A433M cavity-altering mutation. Structural analysis of these stabilized gp120 variants in complex with CD4 and Fab 17b at 2.0-2.2 Å resolution showed that four of five disulfides formed (except 231-268), and that M95W and A433M, in the context of the 96-275 disulfide, induced minimal structural perturbation.

To increase stabilization, we tested disulfide and cavity-altering combinations. Folding difficulties were encountered with combinations of three or four interdomain disulfides (supplementary Table 2). A four-disulfide core did not fold, and only two combination of three disulfides produced adequate levels of folded protein (supplementary Table 2). We analyzed one of these three-disulfide variants with linkages at 96-275, 109-428, and 123-431, bound to CD4 and 17b at 2.8 Å resolution. We also analyzed a two-disulfide variant with linkages at 96-275 and 109-428 at 2.5 Å resolution. In both structures, all potential disulfides formed.

a, Structural details of stabilization. The ribbon diagram depicts the gp120 inner domain (gray), outer domain (red), and bridging sheet (blue), along with stick models of introduced disulfides (with carbon atoms in green) and cavity-altering substitutions (with carbon atoms in magenta). Inset boxes show electron density (2Fo-Fc, contoured at 1σ) corresponding to each mutational substitution. **b**, Unliganded SIV gp120, with polypeptide in ribbon diagram colored the same as **a**. Positions corresponding to introduced cysteines are green, with disulfide connections that only form in the CD4-bound conformation highlighted with yellow dashes and with associated Cα distances. As can be seen, each of the four disulfides is structurally incompatible with the conformation of the unliganded SIV gp120. **c**, Antigenic analysis of conformational stabilization. The vertical axis corresponds to the change in entropy of each particular gp120 variant upon binding to CD4. In the left panel, the horizontal axis corresponds to the on-rate for the CD4-induced (CD4i) antibodies, 17b and m6 (in blue and red, respectively). In the middle panel, the horizontal axis corresponds to the on-rate of CD4. In the right panel, the horizontal axis shows the aggregate change in $\Delta\Delta G$ for the 10 CD4-binding-site (CD4BS) antibodies listed in Table 1. In $\Delta\Delta G$ calculations, a maximal change in affinity of 10^5 was used.

Supplementary Figure 2

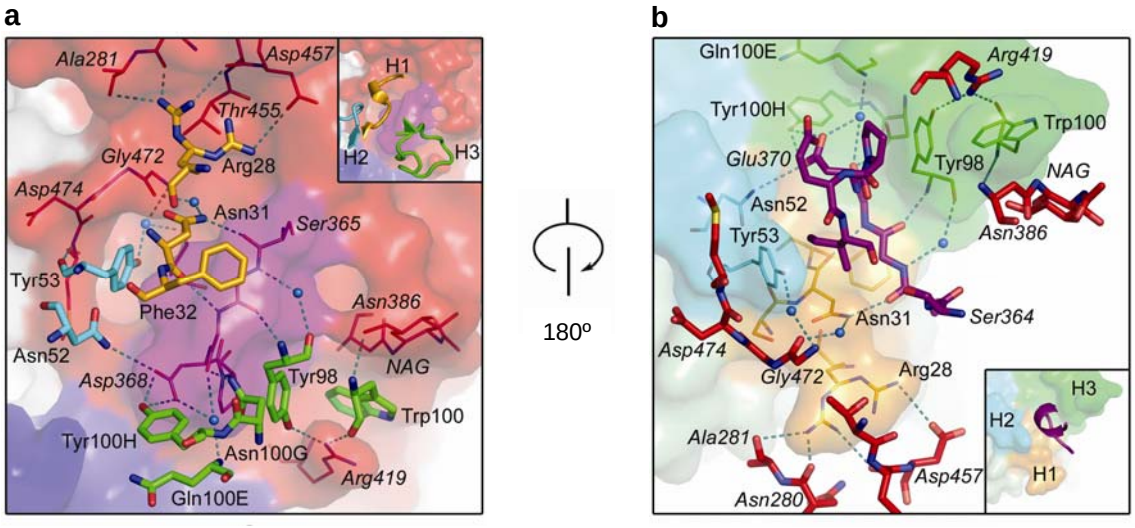

Supplementary Figure 2. Structural details of b12 complexed to an HIV-1 gp120 core.

All three of the heavy chain complementarity-determining regions (CDRs) of b12 make extensive contact with gp120. The CDR H1 (197 Å^2) uses Arg 28 and Asn 31 to make polar interactions, and Phe 32 to pack hydrophobically over the N-terminal portion of the CD4-binding loop (β15-α3 of gp120). The CDR H2 (245 Å^2) inserts between the CD4-binding loop and β20/21, positioning Tyr 53 into a hydrophobic cleft at the C-terminus of the CD4-binding loop. The base of the CDR H3 (276 Å^2) also makes extensive contacts with the CD4-binding loop, with both polar (e.g. three hydrogen bonds) and hydrophobic (e.g. Tyr 98 stacks over gp120 proline residue 369) interactions. Meanwhile, the extended CDR H3 tip projects towards the glycosylated silent face, with Trp 100 at the CDR H3 tip sandwiched between gp120 Arg 419 and Asn 386, which is N-glycosylated (in a rare antibody:glycan interaction, the glycan attached to Asn 386 makes a hydrogen bond to the backbone amide of Trp 100 – "*NAG*" above). Together, these six b12 heavy chain residues, at positions 28, 31, 32, 53, 98, and 100, make up 65% of the b12 contact surface. Mutation to alanine of resides 53, 98 and 100 was previously shown to ablate b12 binding (supplementary Table 6) [Zwick, M. B. et al. *J. Virol.* **77,** 5863-5876 (2003)].

a, Details from a b12 perspective. The gp120 molecular surface is depicted along with specific residues of b12 and gp120 as stick and line models, respectively. The gp120 molecular surface is colored purple for the surface associated with the CD4-binding loop, red for the surface associated with the rest of

the outer domain, gray for the surface associated with the inner domain, and blue for the surface associated with β20/21, which in the CD4-bound conformation form part of the bridging sheet. Stick models are colored according to atom type: carbon atoms are colored orange-yellow (CDR H1), cyan (CDR H2), and green (CDR H3) for b12 and red (outer domain) and purple (CD4-binding loop) for gp120, with nitrogen atoms in blue, oxygen atoms in red, and select water molecules in blue. Atoms involved in hydrogen bonds are connected by dashed lines. Labels specifying gp120 residues are italicized, with those specifying b12 residues in normal script. Arg 28 in the b12 CDR H1 assumes two conformations, both of which are shown. Inset of the same orientation shows the CDR H1, H2 and H3 loops (depicted in ribbon diagram) arrayed around the CD4-binding loop (purple surface). **b**, Details from a gp120 perspective. The orientation has been rotated 180º about a vertical axis. The b12 molecular surface is depicted along with highlighted residues of gp120 and b12 as stick and line models, respectively. The b12 molecular surface is colored orange-yellow for the surface associated with the CDR H1, cyan for the surface associated with the CDR H2, green for the surface associated with the CDR H3, and gray otherwise. Stick models are colored as specified in **a**. Labels specifying gp120 residues are italicized, with those specifying b12 residues in normal script. Inset of the same orientation shows the CDR H1, H2 and H3 surfaces grasping onto the CD4-binding loop, which is displayed as a purple ribbon diagram.

Supplementary Figure 3

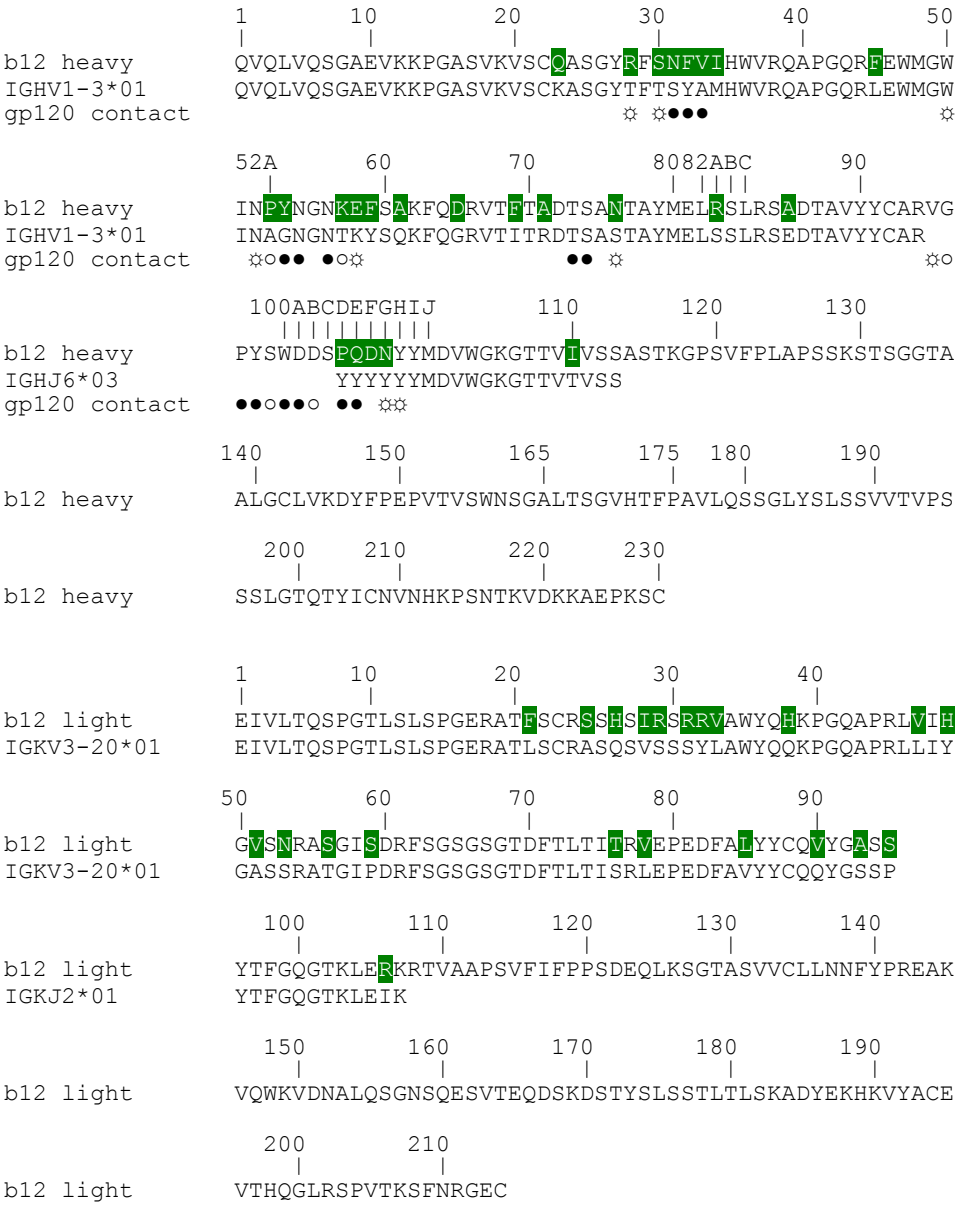

Supplementary Figure 3. Genomic analysis and sequence of b12.

Sequences of the b12 heavy chain and light chain are shown, along with the genomic VH and VL precursor for each chain, and numbered according to Kabat. Positions where the mature b12 sequence differs from the genomic precursor are highlighted with green shading. Contacts of each residue with gp120 as defined in the crystal structure are defined by gp120 mainchain only interaction (open circles), sidechain only interaction (circles with rays), or both sidechain and mainchain interactions (filled circles).

Supplementary Figure 4

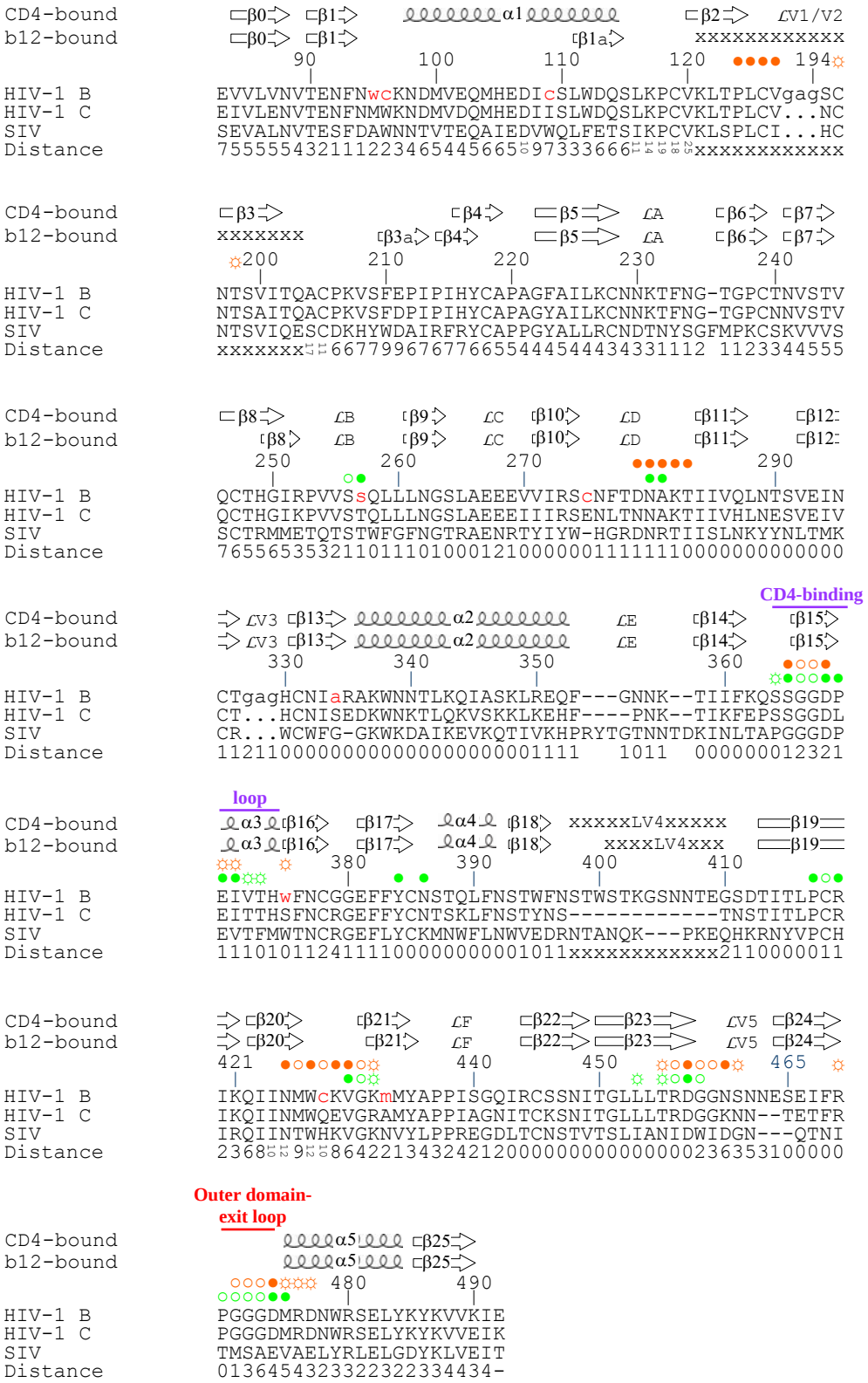

Supplementary Figure 4. gp120 sequence, secondary structure, contact residues, and structural differences between b12- and CD4-bound states.

Sequences of clade B isolate HXBc2 (Ds12F123 core variant), of consensus clade C, and also of SIV_{mac239} are displayed. Sequence numbering follows the HXBc2 convention, with a "gag" tripeptide replacing V1/V2 and V3 excursions. Residues 95, 96, 109, 257, 275, 334, 375, 428 and 433 (in lower case and red) have been substituted from the HXBc2 sequence to make the partially stabilized Ds12F123 variant. Symbols in green and orange-yellow signify gp120 contacts as defined with the program MS [Connolly, M. L. *J. Mol. Graph*. **11**, 139-141 (1993)] for b12 and CD4 complexes, respectively, with open circles denoting only gp120 mainchain contact, open circles with rays denoting only gp120 sidechain contact, and filled circles denoting both mainchain and sidechain contact. "Distance" enumerates the Cα distances between the b12- and CD4-bound structures of gp120 after outer domain superposition. Secondary structural elements for both b12- and CD4-bound conformation are drawn and labeled, according to previously defined convention [Kwong, P. D. et al. *Nature* **393**, 648-659 (1998)]. Regions corresponding to the "CD4-binding loop" (containing secondary structural elements, β15 and α3) and the "outer domain-exit loop" (the loop between β24 and α5) are denoted and labeled in purple and red, respectively.

As expected from the use of the conformationally constrained gp120 in crystallization, the overall b12-bound conformation was similar to that induced by CD4, though with important differences. These differences relate primarily to the regions, which in the CD4-bound state form the bridging sheet, and to proximal portions of the inner domain.

In the bridging sheet (β2, β3, β20 and β21), significant differences were observed between the b12-bound conformation and the unliganded and CD4-bound states. β2 and β3 are not ordered sufficiently in the b12-bound conformation to be resolved. Meanwhile, β20 proceeds in the same direction as the preceding β19, so that in the b12-conformation the β20-β21 ribbon is turned 90º with respect to unliganded and CD4-bound conformations (Fig. 2).

In the inner domain around the core N- and C-termini, the b12 conformation is different from the unliganded state (Cα RMSD of 10.0 Å) and, although similar to the CD4-induced one (Cα RMSD of 4.6 Å), there are notable differences. Thus for example, the 2-on-3 β-sandwich of the termini is retained, though with a rigid body shift of 2.4 Å. The inner domain structural similarity is preserved through the first

turn of the long α1 helix, and then breaks down. Despite the 109-428 disulfide and stabilizing substitutions introduced in residues 257, 375 and 433, this region is considerably different from both the unliganded SIV and CD4-bound HIV-1 states. Indeed, within the inner domain/bridging sheet, only the α5 helix retains its position, and even there, shifts of 2-5 Å are observed. The overall differences demonstrate the flexibility of the inner domain and bridging sheet, even in the presence of multiple substitutions designed to fix gp120 in the CD4-bound state.

The conformation of the outer domain, which serves as the central binding site for b12 and CD4, is remarkably well preserved between unliganded, b12- and CD4-bound states (Fig. 2). This similarity is reflected in a Cα RMSD of only 1.3 Å between outer domains of b12- and CD4-bound states. The differences in outer domain are greater between unliganded SIV gp120 and liganded HIV-1 gp120 (average SIV difference is 4.36 Å). The CD4-binding loop, for example, is significantly different in the unliganded SIV structure and much more similar in b12- and CD4-bound states. Interestingly, the Cα RMSD for residues of the outer domain in contact with b12 and CD4 is 2.0 Å, significantly higher than non-contact residues (Cα RMSD of 1.1 Å) (significance of contact versus non-contact RMSD, $P < 0.0019$), suggesting that the few differences observed in the HIV-1 outer domain are induced by b12 or CD4 binding.

Overall, these results confirm the conformational flexibility in liganded versus unliganded gp120 [Chen, B. et al. *Nature* **433**, 834-841 (2005)]. They highlight the remarkable shape-changing abilities of the inner domain and regions associated with the bridging sheet. The results also highlight the structural invariance of the outer domain.

Supplementary Figure 5

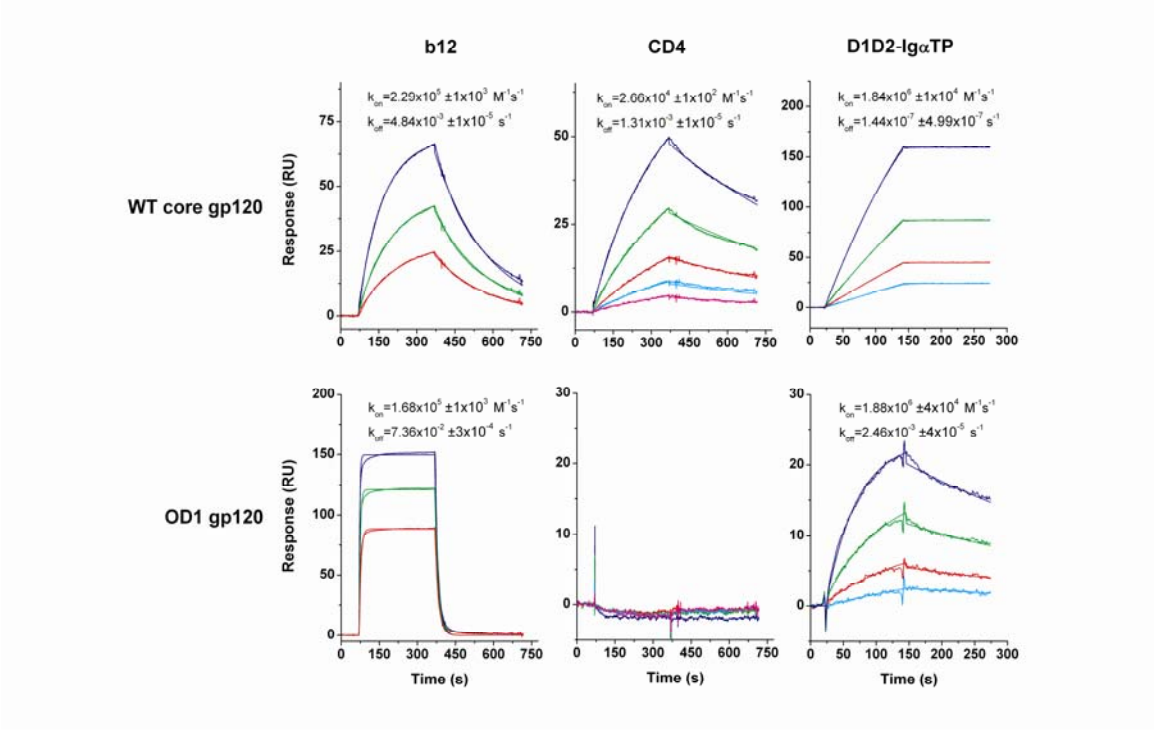

Supplementary Figure 5. Surface-plasmon resonance analysis of b12, CD4 and D1D2-Igαtp interactions with core and outer domain fragment (OD1) of gp120.

CD4 (d1d2) and b12 were directly immobilized onto CM5 sensor chips to surface densities of ~500 response units (RU) with standard amine coupling. Increasing concentrations of gp120 or OD1 were passed over coupled sensor chips at 30 μl/min for 5 min, followed by a 5-min dissociation phase. The buffer in all experiments was 10 mM HEPES, pH 7.4, 150 mM NaCl, 3 mM EDTA, and 0.01% surfactant P-20. Sensorgrams were fit globally with BiaEvaluation 4.1 using a 1:1 Langmuir model of binding. Concentrations of wild-type core gp120 (top row) were 6.2 nM (red), 12.3 nM (green) and 24.6 nM (blue) for b12 (left panel) and 6.2 nM (magenta), 12.3 nM (cyan), 24.6 nM (red), 49.3 nM (green) and 98.5 nM (blue) for CD4 (middle panel). Concentrations of the OD1 fragment of gp120 (bottom row) were 0.38 μM (red), 0.75 μM (green) and 1.5 μM (blue) for b12 (left panel) and 0.38 μM (magenta), 0.75 μM (cyan), 1.5 μM (red), 3.0 μM (green) and 6.0 μM (blue) for CD4 (middle panel). Concentrations of CD4 of up to 0.7 mM were tested, which resulted in increased background, but not reportable binding.

The exploitation of D1D2-Igαtp avidity can only occur if it is the analyte. Wild-type core and OD1 variants of gp120 were immobolized onto CM5 sensor chips at densities of 430 and 385 RU, respectively. To minimize nonspecific binding of D1D2-Igαtp, alcohol dehydrogenase (*S. cerevisiae*, Sigma) was immobilized onto the reference surface and 0.1% carboxymethyl dextran was added to the buffer. Increasing concentrations of D1D2-Igαtp were allowed to bind for 2 min and then to dissociate for 2 min, with a flow rate of 30uL/min. Concentrations of D1D2-Igαtp (right panels) were 0.62 nM (cyan), 1.25 nM (red), 2.50 nM (green) and 5.00 nM (blue) for wild-type core (top row), and 1.25 nM (cyan), 2.50 nM (red), 5.00 nM (green) and 10.0 nM (blue) for OD1 (bottom row).

Supplementary Figure 6

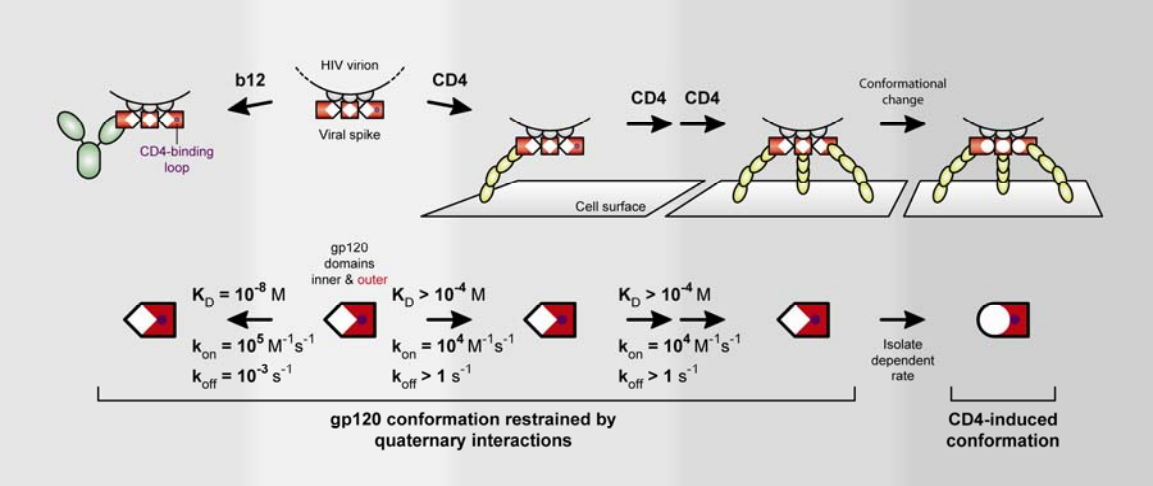

Supplementary Figure 6 Model for CD4 engagement and effective antibody neutralization of HIV-1. In neutralization-resistant isolates, the viral spike is configured with virtually all surfaces occluded by glycan, and only the CD4-binding loop and neighboring surfaces exposed. The b12 antibody is able to bind with high affinity to this loop region, without requiring large conformational rearrangements in gp120. In this manner it bypasses conformational masking, the quaternary restrictions that prevent ligands which require conformational change from binding to gp120 in the context of a functional viral spike. The initial contact of CD4 also occurs with the CD4-binding-loop region, and while its on-rate is similar to that of b12, its off-rate is much faster. The upper schematic depicts the interaction of b12 and cell-surface CD4 with a viral spike. The parallel lower schematic focuses only on gp120, depicting affinity and rates of association and dissociation as determined for b12 and inferred for CD4, from interactions with the outer domain (OD1) (Supplementary Fig. 5). The far right state shows a conformation, induced by CD4, which is less encumbered by quaternary restrictions, and can be bound by many ligands including coreceptor and also the fusion inhibitor T-20; the far left state shows a dead-end complex, the product of b12 binding to the CD4-binding loop of one of the viral spike's gp120 protomers.